Applied Surface Science 538 (2021) 147977

Contents lists available at ScienceDirect

Applied Surface Science

journal homepage: www.elsevier.com/locate/apsusc

More than physical support: The effect of nickel foam corrosion on electrocatalytic performance

Xiuming Bu[a,b,1], Renjie Wei[a,1], Zhengyang Cai[c], Quan Quan[a], Heng Zhang[a,d,e], Wei Wang[a], Fangzhou Li[a], Sen Po Yip[a,d,e], You Meng[a], Kwok Sum Chan[b,e], Xianying Wang[c], Johnny C. Ho[a,d,e,f,*]

[a] Department of Materials Science and Engineering, City University of Hong Kong, Kowloon 999077, Hong Kong Special Administrative Region
[b] Department of Physics, City University of Hong Kong, Kowloon 999077, Hong Kong Special Administrative Region
[c] School of Materials Science and Technology, University of Shanghai for Science and Technology, Shanghai 200093, China
[d] State Key Laboratory of Millimeter Waves, City University of Hong Kong, Kowloon 999077, Hong Kong Special Administrative Region
[e] Centre for Functional Photonics, City University of Hong Kong, Kowloon 999077, Hong Kong Special Administrative Region
[f] Key Laboratory of Advanced Materials Processing & Mold (Zhengzhou University), Ministry of Education, Zhengzhou 450002, China

ARTICLE INFO

Keywords:
Nickel foam
Corrosion
Electrocatalytic
Electrocatalyst
Hydrothemal
Solvothermal

ABSTRACT

Nickle foams (NFs) have been widely used as substrates to support various electrocatalysts due to their extended framework structures, low-cost and high-conductivity. At the same time, as a kind of relatively active metals, nickel substrates are also prone to get corroded or chemically etched during hydro-/solvothermal synthesis of catalyst materials. However, as far as we know, when using NFs as the scaffold to support Ni-free electrocatalysts, most of the published works overlook or even ignore the effect of nickel corrosion on the activities of electrocatalysts directly fabricated on NFs. By using a simple comparison method, we systematically studied such effects from the aspects of material-synthesis temperature, precursors and aqueous solution involved. Our results indicate that the nickel substrates do indeed corrode with ions out-diffused into the reaction solution and incorporated into the fabricated electrocatalysts, which in turn affect their electrocatalytic performances. Special cautions and considerations should be made accordingly when employing nickel foams as substrates for electrocatalysts.

1. Introduction

In the past decades, because of the prominent energy crisis, research and development in the electrochemical energy conversion and storage devices have drawn an extensive attention in the scientific community [1–5]. They include numerous studies in hydrogen evolution reaction (HER), oxygen evolution reaction (OER), oxygen reduction reaction (ORR) and supercapacitors, *etc* [6–9]. All these works aim to explore and design the appropriate low-cost and high-performance electrocatalysts for practical applications. Among many recent advances, it becomes very common to prepare various kinds of electrocatalysts directly onto three-dimensional (3D) substrates, such as Ni foams (NFs), due to their low-cost, large effective surface area and highly conductive continuous porous frameworks [10–17]. The performance of electrocatalysts is generally evaluated by comparing their values of overpotential required and corresponding Tafel slopes resulted when their current density values reach 10 mA cm^{-2}; therefore, a low overpotential and a small Tafel slope are the universal indicators for an efficient catalyst. Using 3D substrates, the fabricated electrocatalysts can further promote their exposed surface area (i.e. active sites) for more efficient catalytic reactions in the electrolyte, since the number of exposed active sites is one of the most important factors contributing to catalytic performance enhancement despite the fact of using geometrical area here, rather than specific surface area, for the performance comparison [18,19].

In fact, the large-scale use of NFs in the electrochemical energy conversion and storage devices can be dated back to 15 years ago, in which NFs were served as the substrate as well as the catalyst in fuel cells [20–24]. It has been widely confirmed that the nickel ions would diffuse out from the nickel foam framework and become dopants to the

* Corresponding author at: Department of Materials Science and Engineering, City University of Hong Kong, Kowloon 999077, Hong Kong Special Administrative Region.
E-mail address: johnnyho@cityu.edu.hk (J.C. Ho).
[1] The authors contributed equally to this work.

https://doi.org/10.1016/j.apsusc.2020.147977
Received 29 June 2020; Received in revised form 28 August 2020; Accepted 22 September 2020
Available online 28 September 2020
0169-4332/

material system since the working environment of fuel cells is always under high temperatures (*e.g.* above 400 °C) [25]. In this case, it seems reasonable that most researchers do not take into a serious consideration for the nickel ion out-diffusion from NFs when HER, OER and other applications are operated in room temperature. Typically, the catalysts are fabricated and supported onto NFs *via* four major methods, which comprise physical loading [26,27], dip coating [28,29], electrodeposition[11,13,30] and hydrothermal deposition [31–33]. As compared with the first three preparation methods, the hydrothermal synthesis is a more popular technique owning to the simple operation procedure, close contact between catalysts and substrates, effective manipulation of different catalyst morphologies and more importantly the low cost. In any case, the hydrothermal synthesis relies heavily on the crystallization process of reaction products from high-temperature precursor solutions (*e.g.* ranging between 120 and 220 °C) at high vapor pressures [34]. These reaction conditions are also considered to be as harsh as the ones of fuel cells. At the same time, there are several latest works focused on the *in-situ* Ni-doped catalysts for electrochemical utilizations. For example, Zhou and his team reported a facile one-step preparation of *in-situ* Ni-doped transition metal oxide (Co, Mn and Fe) nanosheets synthesized on NFs using the hydrothermal method [35]. The doping source of Ni was attributed to the chemical etching of NFs by H^+, which comes from the hydrolysis of metal chloride during the synthesis reaction. In addition, Yao *et al.* also achieved the bifunctional electrocatalysts based on hybrid iron/nickel phosphides fabricated on NFs [36]. It is found that during the hydrothermal synthesis, iron nitrate and nickel foam were employed as the precursor, where nickel ions were evidently resulted from the oxidation reaction between Fe^{3+} ions and nickel foams. These two reports clearly suggest that nickel ions coming from the nickel foams would participate in the reaction throughout the entire process of material synthesis. However, until now, there is still not any systematic investigation on the effect of nickel ion out-diffusion by using NFs as supporting substrates on the electrochemical properties of fabricated electrocatalysts.

Herein, we raise the following three questions in order to investigate the above doubt. First of all, do nickel foams get corroded in blank distilled water during the typical hydrothermal process? Secondly, do precursors and commonly used additives induce any corrosion behavior of the nickel foams? Finally, if corrosion is indeed occurred on the nickel foams, do the out-diffused Ni ions participate freely in subsequent chemical reactions? Answering these three questions would become essential to tackle any issue of using the nickel foams as supporting substrates for electrocatalysts.

2. Materials and methods

2.1. Materials synthesis

In this study, all nickel foam samples were cut into pieces (1.5 × 4 × 0.1 cm), treated with the following cleaning steps: acetone, 2 M HCl, distilled water and ethanol treatment for 10 mins, respectively. In a typical synthesis process, a piece of NF was added into a 15 mL of Teflon-lined stainless-steel autoclave with 10 mL of fresh distilled water (pH = 7.04). Then, the autoclave system was transferred into an oven and kept at 120 °C for 6 h. Four more contrast samples were prepared at other different temperatures. To further illustrate the effects of additives, several kinds of additives were added into the fresh distilled water with the same treatment process, including 50 mg urea (99% ACROS), 1 mmol $Fe(NO_3)_3{\cdot}9H_2O$ (AR, ACROS), 1 mmol $Fe(SO_4)_2{\cdot}7H_2O$ (GR, ACROS), 1 mmol $Co(NO_3)_2{\cdot}6H_2O$ (AR, ACROS) and 1 mmol $MnCl_2{\cdot}4H_2O$ (AR, ACROS).

For cobalt carbonate hydroxide/NFs preparation, 0.5 mmol of $Co(NO_3)_2{\cdot}6H_2O$, 2.5 mmol urea and 1.25 mmol of NH_4F were added into 10 mL distilled water to form a clear solution by stirring for 15 min. After that, the mixture was transferred into a 15 mL glass bottle with a piece of nickel foam (1.6 × 3 × 0.1 cm). Finally, the glass bottle was put in a Teflon-lined stainless-steel autoclave and kept at 120 °C for 6 h. For comparison, the samples treated in 130 °C, 140 °C and 150 °C were also prepared.

2.2. Materials characterization

Powder X-ray diffraction (XRD) was employed to investigate the crystal structure and purity of the samples with a scan rate of 0.05°/s in a 2θ scan ranging from 10° to 90°, using a Bruker D2 Phaser (Bruker, Billerica, MA, USA) instrument equipped with a monochromatized Cu–Kα radiation. The morphologies of the samples were observed by scanning electron microscopy (SEM, Phenom Pro, Phenom-World, The Netherlands) with an accelerating voltage of 10 kV and by field-emission SEM (SU-8010, Hitachi, Tokyo, Japan) with an accelerating voltage of 10 kV. The concentration of Ni ions was measured using an inductively coupled plasma atomic emission spectrometry (PE optima 8000). Transmission electron microscopy (TEM) equipped with EDS were conducted by a Tecnai G^2 F30 (FEI, Hillsboro, OR, USA) using an accelerating voltage of 300 kV. X-ray photoelectron spectroscopy (XPS) was performed with a VG Multilab 2000 (Thermo Fisher Scientific, Waltham, MA, USA) photoelectron spectrometer using a monochromatic Al–Kα radiation under vacuum at a pressure of 2×10^{-6} Pa. All of the binding energies were referenced to the C1s peak at 284.8 eV of the surface adventitious carbon.

2.3. Electrochemical measurement

For electrochemical measurement, the active area of cobalt carbonate hydroxides/NFs for contacting with the electrolyte was defined by applying the silicon rubber. A Gamry 300 electrochemical workstation connected with a standard three-electrode configuration under 25 °C using a constant temperature bath was used to conduct electrochemical characterizations. The fabricated electrode sample was used as the working electrode. A saturated calomel electrode (SCE) and a carbon rod were employed as the reference electrode and counter electrode, respectively. All reported potentials were calibrated versus the reversible hydrogen electrode (RHE) using the equation of $E_{RHE} = E_{SCE} + (0.21 + 0.059 \times pH)$ V, where E_{RHE} is the potential referred to RHE and E_{SCE} is the measured potential against the SCE reference electrode. The activities of OER were surveyed in 1 M KOH aqueous solution (pH = 13.73) by linear sweep voltammetry (LSV) at a scan rate of 10 mV s^{-1}. To keep the electrode surface in a relatively stable state, several cyclic voltammetry (CV) cycles were operated before the assessment of OER activity until the redox peaks and the oxygen evolution currents showed the unnoticeable change. Unless otherwise mentioned, the voltammograms were recorded with the iR drop compensation automatically on the workstation.

3. Results and discussion

Before addressing these matters, it is worth noting that when fresh distilled water is exposed to atmosphere for a long duration, the ambient carbon dioxide would dissolve into water to give the weakly acidic solution, which may substantially affect the experiments performed later. In this regard, fresh distilled water is employed for every single experiment in this study. To begin this investigation, a series of comparative experiments with NFs processed in the blank aqueous solution and typical hydrothermal treatments were first conducted at different temperatures, ranging from 120 °C to 200 °C, for 6 h (see details in Experiment Section). Based on the surface morphologies observed under scanning electron microscopy (SEM), it is evident that the NF samples (processed from 120 °C to 160 °C) have a rough surface together with the existence of etch pits, while the amounts and size of the pits increase with the increasing temperature (Fig. 1a-f). While the temperature exceeds 170 °C, in addition to etch pits, tiny nanowires are found attached on the surface of substrate (Fig. 1g). As the temperature

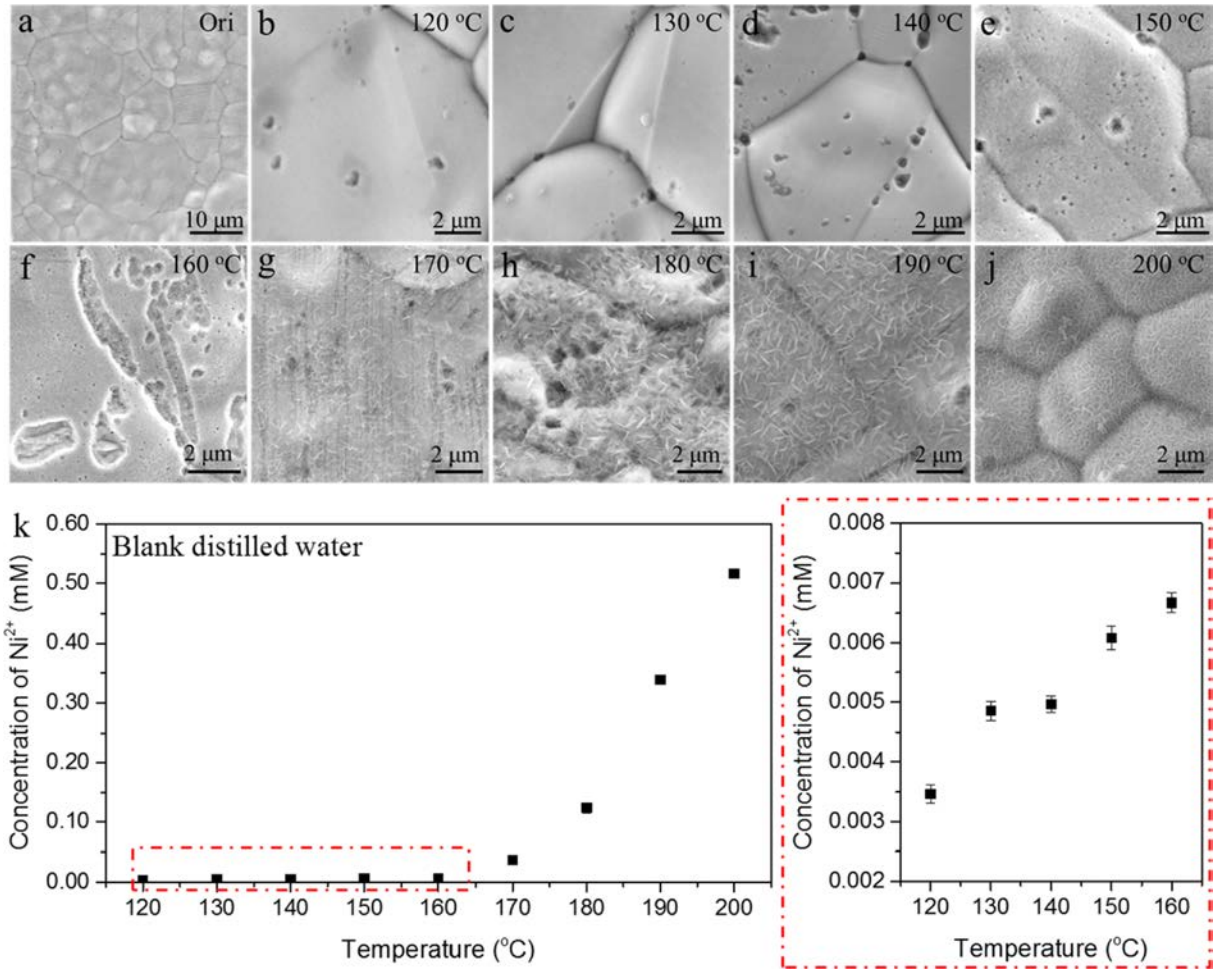

Fig. 1. The corrosion behavior of NFs in the blank aqueous solution at different temperatures during the hydrothermal process. (a-j) SEM images of nickel foams after hydrothermal treatment in the blank aqueous solution; (k) Corresponded ICP AES results.

increases, the coverage area of the nanowires also increases. The nanowires completely cover the surface when the temperature reaches 200 °C. Inductively coupled plasma atomic emission spectroscopy (ICP AES) was then utilized to directly quantify the free Ni ion (Ni^{2+}) concentration in the reaction solution right after the completion of hydrothermal process (Fig. 1k). As anticipated, the concentration of Ni^{2+} ions is found to be insignificant (less than 7×10^{-3} mM) for the process temperature below 160 °C. The existence of Ni^{2+} ions in the blank aqueous solution may be mainly due to the electrochemical corrosion of NFs. On one hand, the nickel and oxygen dissolved in the distilled water would make up the galvanic cell, causing the corrosion of nickel. On the other hand, since the introduction of impurities is inevitable during the industrial production of nickel foam substrates, such as Co, Fe, Cu, Sn, Mg, Pb and Zn, *etc*., some impurities (*e.g.* Sn and Pb) have the higher electrode potential than nickel, also forming a galvanic cell there. This way, the corrosion of nickel is accelerated for the formation of etch pits during hydrothermal process. Simultaneously, as very small amounts of precursors are needed to produce the target catalyst materials with uniform morphologies (*e.g.* ~ 50 mM in reaction solution) [37–39], the effect of this minimal Ni^{2+} ion concentration here is negligible. However, when the temperature is higher than 170 °C, the concentration of Ni^{2+} ions in the solution gets increased exponentially, being possible to undergo subsequent precipitation reaction onto the catalyst. Combined with the weakly alkaline distilled water used in this experiment, the tiny nanowires are therefore obtained for the process temperature larger than 170 °C. In this case, the nickel foams are confirmed to release significant amounts of free Ni^{2+} ions into the reaction solution for high hydrothermal temperatures, where these Ni^{2+} ions would considerably affect the catalyst composition and performance.

Apart from the blank aqueous solution, since precursors, additives and/or their precipitants are utilized for the electrocatalyst preparation, it is also critical to investigate the effect of their presence on the nickel foam substrates during hydrothermal reactions. For most of the time, transparent solutions are needed for the synthesis of catalysts on NFs. In this work, urea (5 mg/mL) is then selected as the representative precipitant and additive participating in the synthesis reaction. Obviously, once the process temperature exceeds 130 °C, sparse nanosheets start to appear on the NF surface (Fig. 2a-f). Higher temperatures result in the increasing density of obtained nanosheets. It is understood that urea would decompose into the NH_4^+ and OH^- ions throughout the hydrothermal process [39,40]. The formation of nanosheets here indicates the chemical reaction occurred between free Ni ions and hydroxyl ions; therefore, $Ni(OH)_2$ nanosheets are deposited on the NF surface. These free Ni ions existed in the reaction solution may come from the etching of NF material by urea. Meanwhile, detailed ICP AES characterization is performed again to confirm the presence of Ni ions in the solution. It is clear that an exponential increase in Ni^{2+} ion concentration is observed (Fig. 2g). Surprisingly, when the temperature is higher than 150 °C, the Ni^{2+} ion concentration can reach up to a value of 1 mM. This substantial Ni^{2+} concentration can definitely not be ignored in the process of electrocatalyst preparation. Therefore, special attentions have to be paid to the etching effect of NF substrates by precipitants and additives during the catalyst synthesis.

Similarly, in order to explore the effect of precursors on NF

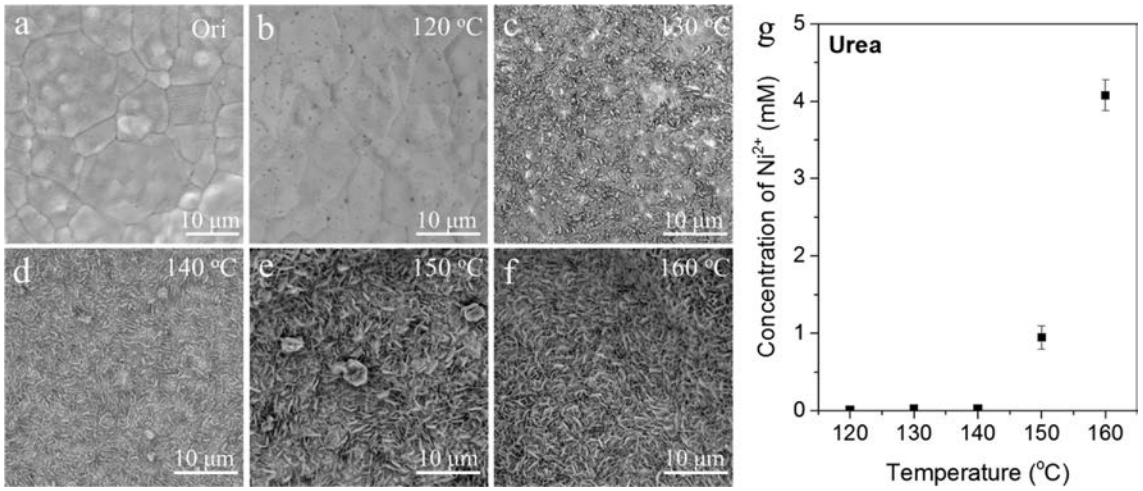

Fig. 2. The corrosion behavior of NFs in the urea solution (5 mg/mL) at different temperatures during the hydrothermal process. (a-f) SEM images and (g) corresponded ICP AES results.

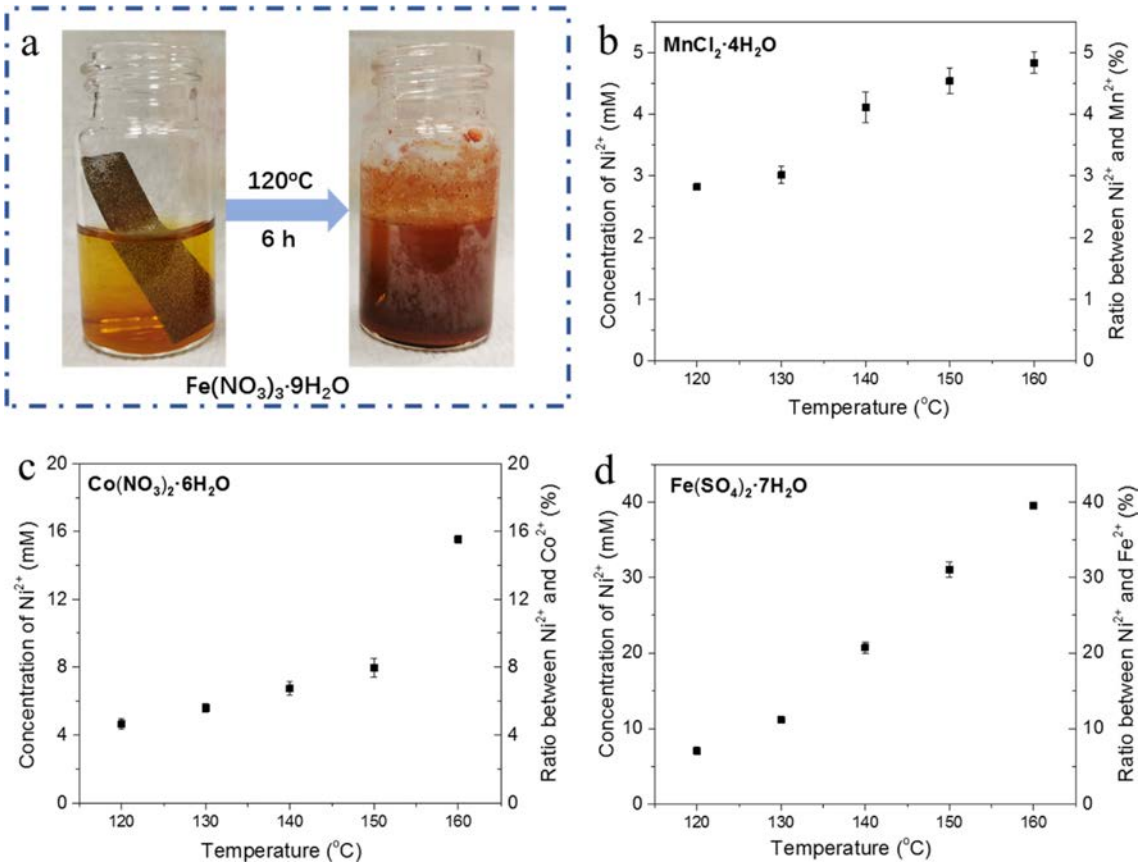

Fig. 3. The influence of different precursors on the NFs, including (a) $Fe(NO_3)_3{\cdot}9H_2O$; (b) $MnCl_2{\cdot}4H_2O$; (c) $Co(NO_3)_2{\cdot}6H_2O$ and (d) $Fe(SO_4)_2{\cdot}7H_2O$.

substrates, several kinds of representative transition metal precursors are employed, including Fe^{3+}, Fe^{2+}, Co^{2+} and Mn^{2+} ions containing species, for the catalyst preparation. For each separate experiment, same amount of precursors (100 mM) are utilized to ensure the fair and consistent study. As shown in Fig. 3a, the introduction of Fe^{3+} ions in the solution induces a strong oxidation–reduction reaction even at a relatively low process temperature of 120 °C. In this particular condition, the NF substrate is completely dissolved in the Fe^{3+} solution. For the cases of other three metal precursors, similar phenomena are also witnessed. It is confirmed that free Ni ions are present in all cases of the solution with the concentration following the sequence of $Fe^{2+} > Co^{2+} > Mn^{2+}$. All show an obvious increase in the Ni ion concentration with the increasing temperatures. Since the hydrolysis of divalent transition metal ions (M^{2+}) is an endothermic reaction ($M^{2+} + 2H_2O \rightleftharpoons M(OH)_2 + 2H^+$, with heat of enthalpy, ΔH greater than 0), the increased temperature favors the reaction to proceed in the forward reaction, which yields the enhanced H^+ ion concentration (Fig. 3b to 3d). This way, the NF substrate would react with H^+ ions and release a large amount of free Ni^{2+} ions in the mixture solution. It is believed that the etching of NFs by Mn^{2+} and Co^{2+} is mostly due to the above-mentioned hydrolysis reaction (Fig. 3b and 3c) while the significantly higher free Ni^{2+} ion concentration obtained in the Fe^{2+} solution is

attributed to the synergistic effect of hydrolysis and strong oxidation-redox reactions (Fig. 3d). In explicit, when we focus on the case of Mn^{2+} (i.e. the one with the lowest Ni^{2+} concentration released), the concentration or mass ratio of between Ni^{2+} and Mn^{2+} ions is already above 2.5% at 120 °C. Hence, the influence of precursors on the NF substrates cannot be carelessly neglected when preparing non-nickel based electrocatalysts.

After confirming the etching effect of transition metal precursors on NF materials, it is evident that nickel foam substrates would contribute considerable influences on the composition and electrochemical properties of electrocatalysts fabricated directly on the substrates. To shed light on the details of these effects on the electrochemical performance of fabricated catalysts, a series of cobalt carbonate hydroxide (CCH) nanomaterials, a typical electrocatalyst for OER, were *in-situ* prepared on the nickel foam with different hydrothermal treatment temperatures. In order to prevent the potential introduction of impurities in the preparation process, a new 15 mL glass bottle was placed in the Teflon-lined stainless steel autoclave (50 mL) as a reaction vessel. The structures of the samples are first investigated by X-ray diffraction (XRD) as shown in Supplementary Information Figure S1. The results illustrate that the change of hydrothermal temperature has no noticeable effect on the crystal structure and phase purity of the CCH, in which they are all consistent with the standard rhodochrosite Co $(CO_3)_{0.5}(OH)\cdot 0.11H_2O$ phase (JCPDS 48–0083) [41]. To ensure the repeatability of the experiment, 5 samples were prepared at each temperature. The SEM observation indicates uniform nanowires being attached onto the NF substrate surface (Supplementary Information Figure S2). Also, the mass loading of CCH catalyst fabricated on the NF substrate is carefully measured by microbalance. With the increasing temperature, the mass loading increases (Fig. 4a). It should be noted that the amount of $Co(NO_3)\cdot 6H_2O$ precursor added in the reaction was precisely controlled. The larger amount of precursor would cause the adsorption of large particles on the substrate, while the smaller amount of precursor makes the catalyst not completely covering the substrate, resulting in the exposure of the nickel foam. All sample preparation details are shown in Experiment Section. Importantly, the thorough TEM observation confirms again the nanowire morphology here (Supplementary Information Figure S3). In this case, all the undesirable circumstances would affect the evaluation of the relationship between hydrothermal temperature and intrinsic electrochemical performance.

Typically, there are three major methods to assess the chemical composition of materials, including ICP AES [12], X-ray photoelectron spectroscopy (XPS) [42] and energy-dispersive X-ray spectroscopy (EDS) [43]. Since it is difficult to separate the CCH catalysts away from the nickel foam substrate completely, EDS may serve as the most applicable technique to evaluate the chemical composition of materials in the current study. Fig. 4b shows the compiled EDS result of atomic ratio between Ni and Co of the prepared samples. When the process temperature increases, the atomic ratio between Ni and Co also gets increased with the value of 11.8 ± 0.6 : 88.2 ± 0.6, 14.3 ± 1.5 : 85.7 ± 1.5, 22.7 ± 1.6 : 77.3 ± 1.6 and 30.3 ± 0.8 : 69.7 ± 0.8 for 120, 130, 140 and 150 °C, respectively. Combined with the XRD result, the relatively high Ni content in the CCH catalysts can be mainly attributed to the absorption of Ni ions on the catalyst since the detection depth of EDS ranges from hundreds of nanometers to micrometers. At the same time, as shown in Fig. 4c, XPS is also employed to investigate whether or not the Ni ions gets doped into the crystal lattice of the catalyst due to the high sensitivity (detection depth is around 10 nm). Considering the catalyst prepared at 120 °C as an example, the peaks located at 781.6 eV and 786.9 eV are attributed to Co $2p_{3/2}$ and satellite peak, respectively. The curve illustrates evidently that the increasing temperature would induce a blue shift in the binding energy of Co, which designates the enhanced doping rate of nickel ions with the higher temperature here, being consistent with the previous results [44]. As the electronegativity of Ni is lower than that of Co, the electron cloud overlapping of Co and O would increase such that Co acquires more electrons; therefore, the doping of Ni ions causes the binding energy of Co to blue shift accordingly. Next, comprehensive

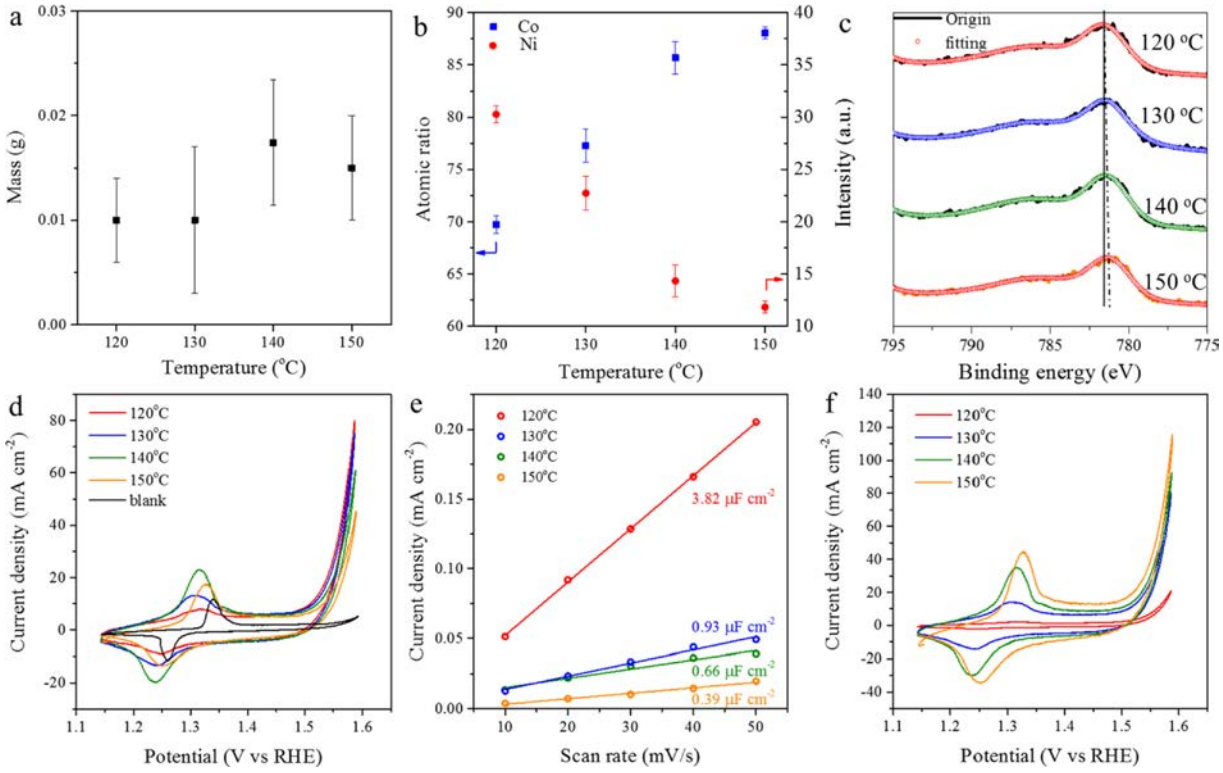

Fig. 4. (a) Mass loading of cobalt carbonate hydroxides on the nickel foam substrates; (b) atomic ratio between Co and Ni obtained from EDS profiles; (c) Co 2p XPS for the samples prepared at different temperatures; (d) OER polarization curves of as-prepared samples with the scan rate of 10 mV s^{-1}; (e) ECSA evaluation from the plots of the current density at 0.05 V vs Ag/AgCl; (f) specific current densities of all samples obtained *via* normalizing the geometric current densities to the ECSA.

electrochemical measurements in a three-electrode configuration with 1 M KOH electrolyte are performed to evaluate the oxygen evolution reaction (OER) characteristics of these different catalysts prepared at different temperatures. All the potentials reported here are referenced to the reversible hydrogen electrode (RHE). As depicted in the original polarization curves of CCH/Nickel foam catalysts, the electrochemical performance decreases with the increasing temperature, where the catalyst prepared at 120 °C delivers the smallest overpotential value and the best performance among all CCH catalysts (Fig. 4d). The electrochemical impedance of the samples prepared at different process temperature show the similar trend (Supplementary Information Figure S4), where the CCH prepared at 120 °C exhibits the smallest charge transfer resistance [45]. It is worth mentioning that the increased temperature actually causes a surface area reduction in nanomaterials [18]. In this manner, the original polarization curve cannot reflect the actual relationship between temperature and intrinsic activity. Electrochemical surface area (ECSA) of all catalyst samples are then determined from their double-layer capacitances (C_{dl}) measured from cyclic voltammetry curves in the range of non-Faraday current at different scanning rates (Supplementary Information S5) [46]. This information is valuable to evaluate the intrinsic electrocatalytic performance of the catalyst. In specific, Fig. 4e shows the extracted relative ECSA values of 3.82 ± 0.04, 0.94 ± 0.06, 0.66 ± 0.07 and 0.39 ± 0.02 for the CCH/Nickel foam catalysts prepared at 120, 130, 140 and 150 °C, respectively. These ECSA results are perfectly consistent with the data trend when compared with the electrochemical characteristics of catalysts as displayed in Fig. 4d. Moreover, the specific current densities of all samples obtained *via* normalizing the geometric current densities to the ECSA are as well presented in Fig. 4f. In contrast with the performance data presented in the original polarization curves, the samples prepared in the 150 °C exhibits the best intrinsic performance, while the intrinsic performance of the samples fabricated in the 120 °C is the worst. Moreover, the TEM and corresponding EDS profiles are also performed on the used catalysts as shown in Supplementary Information Figure S6. The existence of Ni peak on the EDS profiles further confirms the part of Ni comes from the CCH lattice. As a result, all these findings can testify that it is necessary to pay special attentions into the influence of Ni ion out-diffusion as well as their subsequent incorporation into the electrocatalysts when fabricating non-nickel materials directly over nickel foam substrates.

4. Conclusion

In summary, the corrosion behaviors of nickel foams at different conditions during hydrothermal process, including the blank aqueous water, urea as well as Fe^{3+}, Fe^{2+}, Mn^{2+} and Co^{2+} containing solution have been carefully investigated. In addition, the influence of nickel foam substrates on the electrochemical characteristics of non-nickel electrocatalysts have also been evaluated through the performance of cobalt carbonate hydroxides/nickel foam prepared at different hydrothermal temperatures. The increase in temperature leads to an increase in the proportion of nickel doped in the electrocatalyst, which then affects the intrinsic performance. In this case, although the use of nickel foams as substrates is helpful to improve the electrochemical performance of catalysts directly fabricated on the substrates, the nickel foams may contribute free nickel ions to modify the intended catalyst composition and interfere the subsequent analysis of associated catalytic mechanisms. All these alert the community that employment of nickel foams as substrates for electrocatalysts should be very cautious, which is, however, being ignored in the current literature.

5. Credit author statement

Johnny C. Ho conceived and supervised the research. Xiuming Bu and Renjie Wei were responsible for the experiment design and catalyst preparation. Zhengyang Cai, Quan Quan, Heng Zhang, Wei Wang, Fangzhou Li, Yip Sen Po and You Meng performed the experiments and data analysis. Kwok Sum Chan, Xianying Wang and Johnny C. Ho polished the manuscript. All authors discussed the results and commented on the manuscript.

Declaration of Competing Interest

The authors declared that there is no conflict of interest.

Acknowledgment

This work is financially supported by the National Natural Science Foundation of China (Grants 51672229), the General Research Fund (CityU 11211317) and the Theme-based Research (T42-103/16-N) of the Research Grants Council of Hong Kong SAR, China, the Science Technology and Innovation Committee of Shenzhen Municipality (Grant JCYJ20170818095520778) as well as a grant from the Shenzhen Research Institute, City University of Hong Kong.

Appendix A. Supplementary material

Supplementary data to this article can be found online at https://doi.org/10.1016/j.apsusc.2020.147977.

References

[1] Z.W. Seh, J. Kibsgaard, C.F. Dickens, I. Chorkendorff, J.K. Nørskov, T.F. Jaramillo, Combining theory and experiment in electrocatalysis: Insights into materials design, Science 355 (2017) 146–158.
[2] H. Over, Surface chemistry of ruthenium dioxide in heterogeneous catalysis and electro catalysis : from fundamental to applied research, Chem. Rev. 112 (2012) 3356–3426.
[3] M. Shao, Q. Chang, J.-P. Dodelet, R. Chenitz, Recent advances in electrocatalysts for oxygen reduction reaction, Chem. Rev. 116 (2016) 3594–3657.
[4] X. Zou, Y. Zhang, Noble metal-free hydrogen evolution catalysts for water splitting, Chem. Soc. Rev. 44 (2015) 5148–5180.
[5] N.-T. Suen, S.-F. Hung, Q. Quan, N. Zhang, Y.-J. Xu, H.M. Chen, Electrocatalysis for the oxygen evolution reaction: recent development and future perspectives, Chem. Soc. Rev. 46 (2017) 337–365.
[6] N. Han, K.R. Yang, Z. Lu, Y. Li, W. Xu, T. Gao, Z. Cai, Y. Zhang, V.S. Batista, W. Liu, X. Sun, Nitrogen-doped tungsten carbide nanoarray as an efficient bifunctional electrocatalyst for water splitting in acid, Nat. Commun. 9 (2018) 924–934.
[7] Y. Jia, L. Zhang, G. Gao, H. Chen, B. Wang, J. Zhou, M.T. Soo, M. Hong, X. Yan, G. Qian, J. Zou, A. Du, X. Yao, A heterostructure coupling of exfoliated Ni–Fe hydroxide nanosheet and defective graphene as a bifunctional electrocatalyst for overall water splitting, Adv. Mater. 29 (2017) 1700017–1700025.
[8] H. Chen, L. Hu, M. Chen, Y. Yan, L. Wu, Nickel-cobalt layered double hydroxide nanosheets for high-performance supercapacitor electrode materials, Adv. Funct. Mater. 24 (2014) 934–942.
[9] B. Zhang, X. Zheng, O. Voznyy, R. Comin, M. Bajdich, M. García-Melchor, L. Han, J. Xu, M. Liu, L. Zheng, F.P.G. De Arquer, C.T. Dinh, F. Fan, M. Yuan, E. Yassitepe, N. Chen, T. Regier, P. Liu, Y. Li, P. De Luna, A. Janmohamed, H.L. Xin, H. Yang, A. Vojvodic, E.H. Sargent, Homogeneously dispersed multimetal oxygen-evolving catalysts, Science 352 (2016) 333–337.
[10] C. Hu, L. Zhang, Z.J. Zhao, A. Li, X. Chang, J. Gong, Synergism of geometric construction and electronic regulation: 3D Se-(NiCo)S_x/$(OH)_x$ nanosheets for highly efficient overall water splitting, Adv. Mater. 30 (2018) 1705538–1705546.
[11] L. Zhang, P.F. Liu, Y.H. Li, C.W. Wang, M.Y. Zu, H.Q. Fu, X.H. Yang, H.G. Yang, Accelerating neutral hydrogen evolution with tungsten modulated amorphous metal hydroxides, ACS Catal. 8 (2018) 5200–5205.
[12] A. Wu, Y. Xie, H. Ma, C. Tian, Y. Gu, H. Yan, X. Zhang, G. Yang, H. Fu, Integrating the active OER and HER components as the heterostructures for the efficient overall water splitting, Nano Energy 44 (2018) 353–363.
[13] Q. Zhao, J. Yang, M. Liu, R. Wang, G. Zhang, H. Wang, H. Tang, C. Liu, Z. Mei, H. Chen, F. Pan, Tuning electronic push/pull of Ni-based hydroxides to enhance hydrogen and oxygen evolution reactions for water splitting, ACS Catal. 8 (2018) 5621–5629.
[14] Z. Cai, Y. Bi, E. Hu, W. Liu, N. Dwarica, Y. Tian, X. Li, Y. Kuang, Y. Li, X.Q. Yang, H. Wang, X. Sun, Single-crystalline ultrathin Co_3O_4 nanosheets with massive vacancy defects for enhanced electrocatalysis, Adv. Energy Mater. 8 (2018) 1701694–1701702.
[15] L. Zhou, M. Shao, J. Li, S. Jiang, M. Wei, X. Duan, Two-dimensional ultrathin arrays of CoP: electronic modulation toward high performance overall water splitting, Nano Energy 41 (2017) 583–590.
[16] Y. Zhang, B. Wang, F. Liu, J. Cheng, X. wen Zhang, L. Zhang, Full synergistic contribution of electrodeposited three-dimensional NiCo2O4@MnO2 nanosheet networks electrode for asymmetric supercapacitors, Nano Energy. 27 (2016)

627–637.
[17] Z.J. Chen, G.X. Cao, L.Y. Gan, H. Dai, N. Xu, M.J. Zang, H. Bin Dai, H. Wu, P. Wang, Highly dispersed platinum on honeycomb-like NiO@Ni film as a synergistic electrocatalyst for the hydrogen evolution reaction, ACS Catal. 8 (2018) 8866–8872.
[18] S. Sun, H. Li, Z.J. Xu, Impact of surface area in evaluation of catalyst activity, Joule 2 (2018) 1024–1027.
[19] D. Voiry, M. Chhowalla, Y. Gogotsi, N.A. Kotov, Y. Li, R.M. Penner, R.E. Schaak, P.S. Weiss, Best practices for reporting electrocatalytic performance of nanomaterials, ACS Nano 12 (2018) 9635–9638.
[20] S. Freni, G. Calogero, S. Cavallaro, Hydrogen production from methane through catalytic partial oxidation reactions, J. Power Sources 87 (2000) 28–38.
[21] Y. Chen, C. Liu, J.H. Du, H.M. Cheng, Preparation of carbon microcoils by catalytic decomposition of acetylene using nickel foam as both catalyst and substrate, Carbon 43 (2005) 1874–1878.
[22] D.K. Liguras, K. Goundani, X.E. Verykios, Production of hydrogen for fuel cells by catalytic partial oxidation of ethanol over structured Ni catalysts, J. Power Sources 130 (2004) 30–37.
[23] X.E. Hu, H.W. Yang, X.J. Wang, R.S. Bai, Electrohydrogenation of 4-amino-5-nitrosodimethyluracil with a foamed nickel cathode, J. Appl. Electrochem. 32 (2002) 321–328.
[24] J.M. Skowroński, A. Ważny, Nickel foam-based composite electrodes for electrooxidation of methanol, J. Solid State Electrochem. 9 (2005) 890–899.
[25] S.K. Tiwari, Effects of Ni, Fe, Cu, and Cr substitutions for Co in $La_{0.8}Sr_{0.2}CoO_3$ on electrocatalytic properties for oxygen evolution, J. Electrochem. Soc. 143 (1996) 1505–1510.
[26] H.S. Han, Y.R. Hong, J. Woo, S. Mhin, K.M. Kim, J. Kwon, H. Choi, Y.C. Chung, T. Song, Electronically double-layered metal boride hollow nanoprism as an excellent and robust water oxidation electrocatalysts, Adv. Energy Mater. 9 (2019) 1803799–1803810.
[27] Y. Sim, S.J. Kim, G. Janani, Y. Chae, S. Surendran, H. Kim, S.Y.D.C. Seok, Yong Ho Jung, C. Jeon, J. Moon, U. Sim, The synergistic effect of nitrogen and fluorine co-doping in graphene quantum dot catalysts for full water splitting and supercapacitor, Appl. Surf. Sci. 507 (2020) 145157–145165.
[28] G. Dong, M. Fang, J. Zhang, R. Wei, L. Shu, X. Liang, S. Yip, F. Wang, L. Guan, Z. Zheng, J.C. Ho, In situ formation of highly active Ni-Fe based oxygen-evolving electrocatalysts via simple reactive dip-coating, J. Mater. Chem. A 5 (2017) 11009–11015.
[29] F. Li, J. Du, X. Li, J. Shen, Y. Wang, Y. Zhu, L. Sun, Integration of FeOOH and zeolitic imidazolate framework-derived nanoporous carbon as an efficient electrocatalyst for water oxidation, Adv. Energy Mater. 8 (2018) 1702598–1702603.
[30] S.M. Pawar, B.S. Pawar, P.T. Babar, A.T.A. Ahmed, H.S. Chavan, Y. Jo, S. Cho, J. Kim, B. Hou, A.I. Inamdar, S.N. Cha, J.H. Kim, T.G. Kim, H. Kim, H. Im, Nanoporous $CuCo_2O_4$ nanosheets as a highly efficient bifunctional electrode for supercapacitors and water oxidation catalysis, Appl. Surf. Sci. 470 (2019) 360–367.
[31] K. Yan, Y. Lu, Direct growth of MoS_2 microspheres on Ni foam as a hybrid nanocomposite efficient for oxygen evolution reaction, Small 12 (2016) 2975–2981.
[32] X. Zhang, J. Li, Y. Yang, S. Zhang, H. Zhu, X. Zhu, H. Xing, Y. Zhang, B. Huang, S. Guo, E. Wang, $Co_3O_4/Fe_{0.33}Co_{0.66}P$ interface nanowire for enhancing water oxidation catalysis at high current density, Adv. Mater. 1803551 (2018) 1803551–1803559.
[33] H. Xu, J. Wan, H. Zhang, L. Fang, L. Liu, Z. Huang, J. Li, X. Gu, Y. Wang, A new platinum-like efficient electrocatalyst for hydrogen evolution reaction at all pH: single-crystal metallic interweaved V_8C_7 networks, Adv. Energy Mater. 8 (2018) 1800575–1800582.
[34] J. Lai, W. Niu, R. Luque, G. Xu, Solvothermal synthesis of metal nanocrystals and their applications, Nano Today 10 (2015) 240–267.
[35] L. Zeng, K. Zhou, L. Yang, G. Du, L. Liu, W. Zhou, General approach of in situ etching and doping to synthesize a nickel-doped MxOy (M = Co, Mn, Fe) nanosheets array on nickel foam as large-sized electrodes for overall water splitting, ACS Appl. Energy Mater. 1 (2018) 6279–6287.
[36] X. Xu, X. Tian, Z. Zhong, L. Kang, J. Yao, In-situ growth of iron/nickel phosphides hybrid on nickel foam as bifunctional electrocatalyst for overall water splitting, J. Power Sources 424 (2019) 42–51.
[37] W.K. Gao, J.F. Qin, K. Wang, K.L. Yan, Z.Z. Liu, J.H. Lin, Y.M. Chai, C.G. Liu, B. Dong, Facile synthesis of Fe-doped Co_9S_8 nano-microspheres grown on nickel foam for efficient oxygen evolution reaction, Appl. Surf. Sci. 454 (2018) 46–53.
[38] L. Qian, Y. Miao, Nanosheet organized flower-like Co/Zn phosphate on nickel foam for efficient water splitting in both acid and basic solutions, Polyhedron 160 (2019) 213–218.
[39] X. Liang, R. Dong, D. Li, X. Bu, F. Li, L. Shu, R. Wei, J.C. Ho, Coupling of nickel boride and $Ni(OH)_2$ nanosheets with hierarchical interconnected conductive porous structure synergizes the oxygen evolution reaction, ChemCatChem 10 (2018) 4555–4561.
[40] M.L. Kieke, J.W. Schoppelrei, T.B. Brill, Spectroscopy of hydrothermal reactions. 1. The CO_2-H_2O system and kinetics of urea decomposition in an FTIR spectroscopy flow reactor cell operable to 725 K and 335 bar, J. Phys. Chem. 100 (1996) 7455–7462.
[41] Y. Zhang, B. Cui, O. Derr, Z. Yao, Z. Qin, X. Deng, J. Li, H. Lin, Hierarchical cobalt-based hydroxide microspheres for water oxidation, Nanoscale. 6 (2014) 3376–3383.
[42] W. Wang, L. Kuai, W. Cao, M. Huttula, S. Ollikkala, T. Ahopelto, A.P. Honkanen, S. Huotari, M. Yu, B. Geng, Mass-production of mesoporous $MnCo_2O_4$ spinels with manganese(IV)- and cobalt(II)-rich surfaces for superior bifunctional oxygen electrocatalysis, Angew. Chemie - Int. Ed. 56 (2017) 14977–14981.
[43] C. Hu, Q. Ma, S.F. Hung, Z.N. Chen, D. Ou, B. Ren, H.M. Chen, G. Fu, N. Zheng, In situ electrochemical production of ultrathin nickel nanosheets for hydrogen evolution electrocatalysis, Chem. 3 (2017) 122–133.
[44] L. Li, Q. Xu, Y. Zhang, J. Li, J. Fang, Y. Dai, X. Cheng, Y. You, X. Li, Low Ni-doped Co_3O_4 porous nanoplates for enhanced hydrogen and oxygen evolution reaction, J. Alloy. Compd. 823 (2020) 2–7.
[45] Hyunkyu Kim, et al., Fabrication of An Ingenious Metallic Asymmetric Supercapacitor by The Integration of Anodic Iron Oxide and Cathodic Nickel Phosphide, Appli. Surf. Sci. 511 (2020) 145424–145433.
[46] S. Anantharaj, S. Kundu, Do the evaluation parameters reflect intrinsic activity of electrocatalysts in electrochemical water splitting? ACS Energy Lett. 4 (2019) 1260–1264.